A single-crystal magnetization and neutron scattering investigation of the magnetic structure of U_2Rh_2Sn

1996 J. Phys.: Condens. Matter 8 11167

(http://iopscience.iop.org/0953-8984/8/50/039)

J. Phys.: Condens. Matter **8** (1996) 11167–11179. Printed in the UK

A single-crystal magnetization and neutron scattering investigation of the magnetic structure of U_2Rh_2Sn

L C J Pereira†, J A Paixão‡[+], P Estrela§, M Godinho§, F Boudarot‖, M Bonnet‖, J Rebizant†, J C Spirlet† and M Almeida¶

† European Commission, Joint Research Centre, Institute for Transuranium Elements, Postfach 2340, D-76125 Karlsruhe, Germany

‡ Departamento de Física, Faculdade de Ciências e Tecnologia, Universidade de Coimbra, P-3000 Coimbra, Portugal

§ Departamento de Física, Faculdade de Ciências da Universidade de Lisboa, Campo Grande, Edifício C1, P-1700 Lisboa, Portugal

‖ CEA, Departement de Recherche Fondamentale sur la Matière Condensée, SPSMS, F-38054 Grenoble Cédex 9, France

¶ Instituto Tecnológico e Nuclear, Estrada Nacional 10, P-2686 Sacavém Codex, Portugal

Received 8 May 1996, in final form 12 August 1996

Abstract. U_2Rh_2Sn is a member of a large family of intermetallic compounds with the tetragonal U_3Si_2 crystal structure. It orders antiferromagnetically at 28 K with the propagation vector $\boldsymbol{k} = (0, 0, 1/2)$. We have performed magnetization and neutron scattering experiments on a single crystal that show that the uranium atoms order in the collinear Γ_8 irreducible representation of the magnetic group, with the moments aligned parallel to the unique tetragonal axis. The value of the ordered magnetic moment of the uranium atoms refined from the neutron scattering intensities is 0.53(2) μ_B. This is considerably reduced from the free-ion value for both U^{3+} and U^{4+} configurations and suggests that the f electrons are strongly hybridized with the conduction band.

1. Introduction

The electronic and magnetic properties of actinide intermetallics have been the subject of much research, mainly motivated by the intriguing phenomenon known as 'heavy-fermion behaviour' exhibited by some of these compounds. The systematic study of groups sharing the same crystallographic structure can provide relevant information on the electronic structure of actinide intermetallics, especially on the role of the 5f electrons in the bonding (Sechovsky and Havela 1988). In particular, the effect of the hybridization between the 5f electron states and the d and p electron wave-functions of the ligands on the magnetic ground state has received much attention, both as regards theory and experiment.

The ternary U_2Rh_2Sn compound is member of the recently discovered An_2T_2X family (An = U, Np, Pu, Am; T = transition metal; X = p element) which crystallizes in the tetragonal U_3Si_2 type of structure (space group $P4/mbm$) (Péron *et al* 1993, Mirambet *et al* 1993, Pereira *et al* 1995). Bulk measurements on this family of compounds indicate a large variety of electronic and magnetic behaviour; many of them have heavy-fermion properties (Havela *et al* 1995, Nakotte *et al* 1994, Fukushima *et al* 1995). This has been interpreted

[+] Author to whom any correspondence should be addressed.

0953-8984/96/5011167+13$19.50

in terms of the relative importance of the 5f–ligand hybridization along the series and this issue has also been addressed theoretically (Divis *et al* 1994, 1995). Another point that has been a subject of controversy is that of whether the magnetocrystalline anisotropy of these compounds depends upon the shortest distance between the actinide atoms. In fact, a peculiarity of this family of compounds is that the shortest interactinide distance can be found either within the basal plane or along the unique tetragonal axis ($\boldsymbol{c}$), depending on the ligand T and X elements. In the case of U_2Rh_2Sn, the shortest U–U distance is found along the $\boldsymbol{c}$-axis. The general rule that the 5f moments tend to point perpendicularly to the shortest f–f bonds seems to hold for the UTX family. However, neutron diffraction studies have found evidence for strong anisotropic f–d bonding in these systems that could also be responsible for the huge magnetocrystalline anisotropy found in the 1:1:1 system (Paixão *et al* 1992, 1993).

Although a large amount of work has already been reported on the An_2T_2X family, it has unfortunately been restricted up to now to polycrystalline samples. In many cases this rendered it impossible to make a definite statement about the magnetocrystalline anisotropy of these compounds—also because no saturation of the moments in high-field measurements has been observed in most cases.

This work reports the results of magnetization measurements and neutron scattering experiments performed on a single crystal of U_2Rh_2Sn. Previous susceptibility and electrical resistivity measurements on polycrystalline samples have indicated that this compound orders antiferromagnetically with a Néel temperature of 24 K. The possible antiferromagnetic ground state was confirmed by the observation of a field-induced step in high-field magnetization measurements of about 0.3 μ_B/FU occurring at about 20 T (Nakotte *et al* 1994, Fukushima *et al* 1995). Recently Nakotte *et al* (1996) reported a neutron powder diffraction experiment on this compound that confirmed the antiferromagnetic ground state of U_2Rh_2Sn and identified the propagation vector of the magnetic structure as $\boldsymbol{k} = (0, 0, 1/2)$. Unfortunately, this experiment could not determine the magnetic structure unambiguously, because of the limited amount of magnetic scattering observed in the powder diffraction pattern at low temperature. In fact, only two magnetic reflections with significant intensity could be measured. With our measurements performed on a single crystal we could determine the magnetic structure of U_2Rh_2Sn and therefore clarify the present situation concerning the type of magnetic anisotropy found in this compound.

2. Crystal growth and magnetization

The compound U_2Rh_2Sn has been synthesized by arc melting stochiometric amounts of metals under a purified argon atmosphere. The solidified molten sample ($\pm$20 g) was encapsulated in a tungsten crucible sealed by electron beam welding under vacuum (2×10^{-5} atm). The crystals were grown by a modified mineralization technique: we used a radio-frequency-heated crucible allowing the determination of the melting point of the material *in situ* during the crystal growth process, resulting in a shorter time of mineralization (6 h) than is usual. The crystals used for the magnetization and neutron scattering measurements came from the same batch.

Magnetization measurements were performed on a small single crystal of 13.9 mg in mass (approximate dimensions $2.0 \times 1.3 \times 0.9$ mm^3) using a SQUID magnetometer in the temperature range 2–150 K for fields up to 5.5 T applied along the main crystallographic directions.

The temperature dependence of the magnetization for a field of 0.05 T applied along the $\boldsymbol{c}$- and $\boldsymbol{a}$-axes is shown in figure 1(a). The sample was previously cooled in zero field

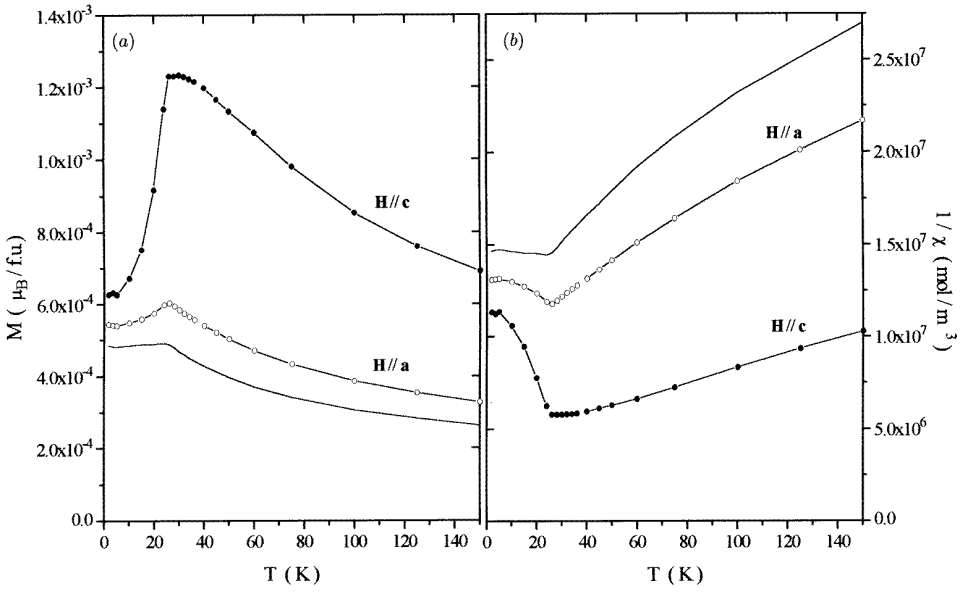

Figure 1. The temperature dependence of the magnetization (*a*) and the inverse susceptibility (*b*) for a field of 0.05 T applied along: $\boldsymbol{c}$ (solid symbols) and $\boldsymbol{a}$ (open symbols). The line represents the corrected magnetization curve for $\boldsymbol{H} \parallel \boldsymbol{a}$ assuming a misalignment of 5° between the $\boldsymbol{a}$-axis and the applied-field direction.

to 2K, after which the field was applied and the $M(T)$-points measured while increasing the temperature. In both directions a well defined peak in the susceptibility is seen corresponding to an antiferromagnetic transition with a Néel temperature $T_N = 28(2)$ K. This value of the Néel temperature is in agreement with the neutron scattering data and is slightly higher than the ones reported from magnetization data for polycrystalline samples ($T_N = 25$ K) (Mirambet *et al* 1994).

The magnetization values observed in the $\boldsymbol{H} \parallel \boldsymbol{a}$ configuration are smaller than the ones in the $\boldsymbol{c}$-direction over the whole temperature range studied, clearly showing that the unique tetragonal axis is the easy axis of magnetization. This is expected for a uniaxial magnetic structure with the moments aligned along the $\boldsymbol{c}$-axis. A uniaxial magnetic structure for U_2Rh_2Sn was suggested by Nakotte *et al* (1996) from specific heat and resistivity measurements and it also gave the best fit to the low-temperature neutron scattering measurements performed by these authors on polycrystalline samples. As shown below, this was also confirmed by our neutron scattering measurements on single crystal. It should be pointed out that the small peak at T_N observed in the susceptibility curve with the field applied along the $\boldsymbol{a}$-axis may be due to a small misalignment of the crystal with respect to the magnetic field direction. In fact, if one considers a misalignment of 5° between the field direction and the $\boldsymbol{a}$-axis, the magnetization becomes almost constant for temperatures up to T_N and the peak is much reduced (figure 1(*a*)).

An analysis of the susceptibility curve for $T > 45$ K shows that there is an important magnetic anisotropy even in the paramagnetic region. For fields applied along the direction of the magnetic moments ($\boldsymbol{H} \parallel \boldsymbol{c}$), a Curie–Weiss behaviour is detected for temperatures above T_N (figure 1(*b*)), with $\theta = -105(2)$ K and an effective Bohr magneton number per uranium atom $\mu_{eff} = 2.80\ \mu_B/U$. In the perpendicular direction ($\boldsymbol{H} \parallel \boldsymbol{a}$), the thermal

variation of the inverse susceptibility shows a positive curvature for the higher temperatures in the paramagnetic region (figure 1(*b*)), well fitted with a modified Curie–Weiss law: $\chi = \chi_0 + C/(T-\theta)$ with $\theta = -60(2)$ K, $\mu_{eff} = 1.34\ \mu_B$/U and $\chi_0 = 1.9\times10^{-8}$ m^3 mol^{-1}.

The data on polycrystalline samples were fitted with a modified Curie–Weiss law with $\theta = -106$ K, $\mu_{eff} = 2.4\ \mu_B$/U and $\chi_0 \approx 1\times10^{-8}$ m^3 mol^{-1} (Havela *et al* 1995). In general, the value of μ_{eff} in polycrystalline samples is expected to be smaller than that obtained along the easy direction of a single crystal, and the modified Curie–Weiss behaviour is often found for polycrystalline samples in systems with high anisotropy in the paramagnetic regime. The modified Curie–Weiss law observed for our single crystal for the measurements along the $\boldsymbol{a}$-axis could be due to a small misalignment of the crystal with respect to the direction of the field, which leads to an additional contribution from the $\boldsymbol{c}$-axis to the total magnetization measured. Therefore, the small value of μ_{eff} that was found for $\boldsymbol{H} \parallel \boldsymbol{a}$ should be treated with caution. An accurate measurement of μ_{eff} along the hard axis will need a better-aligned crystal and extension of measurements to higher temperatures.

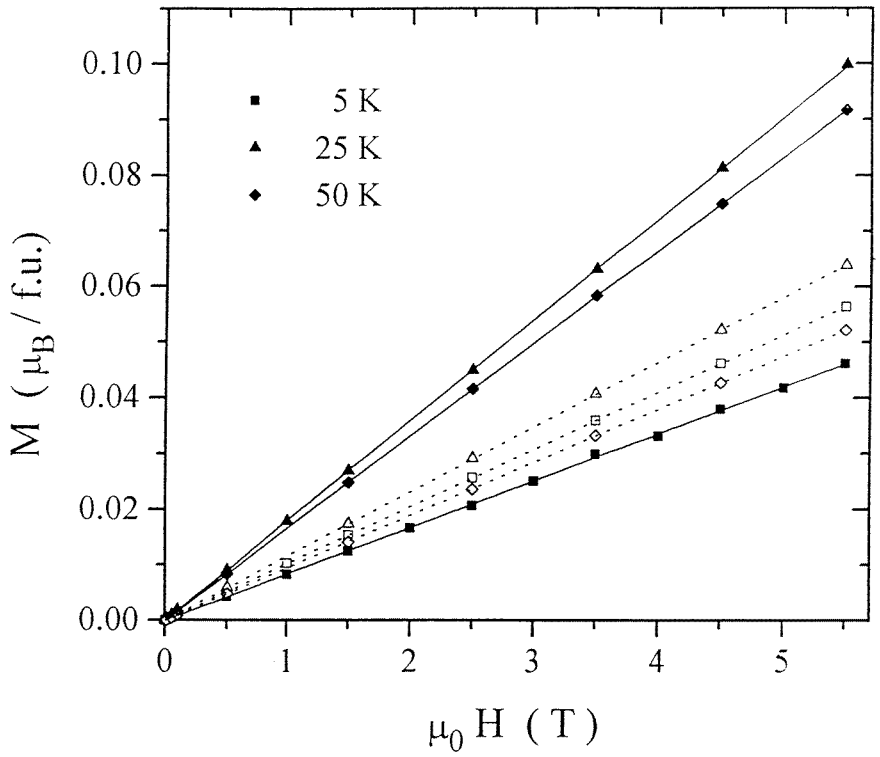

Figure 2. The field dependence of the magnetization at 5, 25 and 50 K (solid symbols: $\boldsymbol{H} \parallel \boldsymbol{c}$; open symbols: $\boldsymbol{H} \parallel \boldsymbol{a}$).

The $M(H)$-curves (figure 2) show a linear behaviour for fields up to 5.5 T in both directions ($\boldsymbol{H} \parallel \boldsymbol{c}$ and $\boldsymbol{H} \parallel \boldsymbol{a}$). The susceptibility ($\mathrm{d}M/\mathrm{d}H$) obtained from the slope of the magnetization curves is also consistent with an antiferromagnetic transition between 25 and 30 K, with the moments aligned along the $\boldsymbol{c}$-axis. No hysteresis was observed for either direction over the whole temperature range studied.

3. Neutron scattering

The neutron scattering experiments were performed at the Siloë reactor of the Centre d'Études Nucleaires de Grenoble, France, on a single crystal with approximate dimensions $2.0 \times 3.5 \times 0.8$ mm^3 . In spite of the absence of well defined crystal faces, metallographic analysis and the neutron scattering experiments on this crystal proved that it consists of a single grain. Two neutron diffraction experiments were performed. In order to refine the crystallographic structure, check the stoichiometry and determine the amount of extinction in our crystal we conducted a preliminary crystallographic study at room temperature on a four-circle diffractometer. For the investigation of the magnetic structure a second experiment was performed at low temperature on a two-axis diffractometer equipped with a He-flow cryostat capable of reaching a temperature of 1.5 K.

3.1. Experimental procedure

A set of 1625 integrated intensities were measured at room temperature on the DN4 four-circle difractometer. A wavelength of 1.1798 Å was selected from the thermal beam by Bragg reflection from a curved Cu(200) monochromator. The measured $\lambda/2$ contamination was $\approx 5 \times 10^{-3}$ of the primary beam intensity. The cell parameters were refined from the UB matrix using a set of 25 strong and well centred reflections within the range $18 \leqslant 2\theta \leqslant 60^\circ$. The values obtained ($a = 7.548(16)$ Å, $c = 3.632(5)$ Å) are in good agreement with those given by neutron powder diffraction data (Nakotte *et al* 1996). The data set extended out to $(\sin\theta)/\lambda = 0.60$ Å^{-1} and for each unique reflection at least three equivalent reflections were measured. A set of two standard reflections were measured every 3 h to monitor the stability of the experimental conditions. Integrated intensities were extracted from the scan profiles using the Lehmann–Larson algorithm (Lehmann and Larson 1974) and corrected for the Lorentz factor. An excellent internal agreement factor between the intensities of equivalent reflections was obtained, $R_I = \sum |I - \langle I \rangle| \sum I = 0.014$, which confirmed the good quality of the data collection and the absence of effects such as anisotropic extinction. No absorption correction was made. After averaging symmetry-equivalent reflections a data set of 197 independent observations with $I > 3\sigma$ were obtained and used for the least-squares refinement of the crystallographic structure.

For the low-temperature work the sample was transferred to the DN3 two-axis normal-beam diffractometer that is equipped with a standard ILL 'orange' cryostat. The sample was mounted with the [140] axis approximately vertical. A neutron beam of wavelength 1.54 Å monochromated by a PG(002) monochromator was used for this study. A pyrolytic graphite filter was inserted in the neutron beam path in front of the sample to reduce the $\lambda/2$ contamination of the beam. Integrated intensities were measured using ω-scans.

3.2. Crystallography

Least-squares refinements of the structural parameters at room temperature were performed using all of the independent reflections with $I > 3\sigma$ (197 observations) starting from the atomic positions of the powder diffraction results of Nakotte *et al* (1996). A locally modified version of the least-squares program SFLSQ (Brown and Matthewman 1987) was used in the calculations. The function minimized in the least-squares procedure was $\sum w(|F_o| - |F_c|)^2$, where $|F_o|$ and $|F_c|$ are the observed and calculated scattering amplitudes, respectively, and $w = 1/\sigma^2$ the weight assigned to each reflection. The variance of the intensities assigned to each reflection was $\sigma_I^2 = \sigma_S^2 + (pF_o^2)^2$ (McClandish *et al* 1975), σ_S^2 being the variance

based on counting statistics and $p = 0.01$ accounting for the instrumental instability down-weighting the strongest reflections. Neutron coherent scattering lengths were taken from the compilation of Koester *et al* (1991): $b_U = 8.417$ fm, $b_{Rh} = 5.88$ fm, $b_{Sn} = 6.226$ fm. An isotropic extinction correction with a Lorentzian mosaic distribution was included in the refinements, but it was found that the extinction was small in our crystal. At $\lambda = 1.178$ Å, the maximum intensity loss due to extinction was $y = 0.74$; the average intensity loss for the measured data set was $\langle y \rangle = 0.97$. The half-width at half-maximum of the Lorentzian mosaic distribution refined in the least-squares procedure converged to the relatively large value of $\eta = 2.25 \times 10^{-4}$ rad $(0.77')$. Atomic positions (x_U, x_{Rh}), anisotropic thermal parameters, one extinction parameter (η), one scale factor and the site occupancies of Rh and Sn were refined (14 variables). The refinement converged within a few cycles to the residual factors $R(F) = 0.022$, $R_w(F) = 0.023$. The final values of the refined structural parameters are given in table 1. They are in very good agreement with the results of the Rietveld refinement on a polycrystalline sample reported by Nakotte *et al* (1996), and also agree well with the results of an x-ray diffraction experiment that we performed on a small single crystal.

Table 1. Positional parameters and anisotropic displacement parameters (in units of 10^4 Å^2), defined as $T = \exp\left[-2\pi^2(h^2a^{*2}U_{11} + \cdots + 2hka^*b^*U_{12} + \cdots)\right]$.

	x	y	z	U_{11}	U_{22}	U_{33}	U_{12}	Site
U	0.172 38(7)	$x + 1/2$	1/2	79(3)	$=U_{11}$	67(4)	0(2)	1.00
Rh	0.367 37(11)	$x + 1/2$	0	99(4)	$=U_{22}$	148(6)	−6(3)	1.01(1)
Sn	0	0	0	74(5)	$=U_{22}$	127(7)	0	1.01(1)

3.3. Magnetism

In agreement with the powder diffraction measurements of Nakotte *et al* (1996) magnetic scattering was found at the reciprocal-lattice positions $(h, k, l) \pm (0, 0, 1/2)$ below 30 K, confirming that the magnetic unit cell is doubled in the *c*-direction compared to the nuclear one. The intensity of the magnetic reflection $(1, 1, 1/2)$ was followed as a function of temperature in the range 1.9 to 35 K (figure 3). A fit of the power law $I/I_0 = (1 - T/T_N)^{2\beta}$ near T_N gives $T_N = 30.0(5)$ K, and $\beta = 0.28(3)$. Such a value of β is consistent with most three-dimensional systems such as Heisenberg or Ising ones. The transition temperature is slightly higher than that found for both the single-crystal susceptibility measurements and in the literature for polycrystalline samples. This small difference has been found to be due to a poor calibration of the thermometer installed on the DN3 cryostat.

The intensities of all magnetic Bragg reflections out to $(\sin\theta)/\lambda = 0.4$ Å^{-1} accessible within the constraints of the normal-beam geometry of the DN3 diffractometer were measured at a stabilized temperature of 1.9 K. After averaging symmetry-related reflections, a unique set of 14 reflections with $I > 3\sigma$ were obtained. These intensities are given in table 2.

3.4. Magnetic structure

Neutron scattering determination of magnetic structures can often take advantage of the tools offered by group-theory analysis, which is very effective in sorting out the magnetic

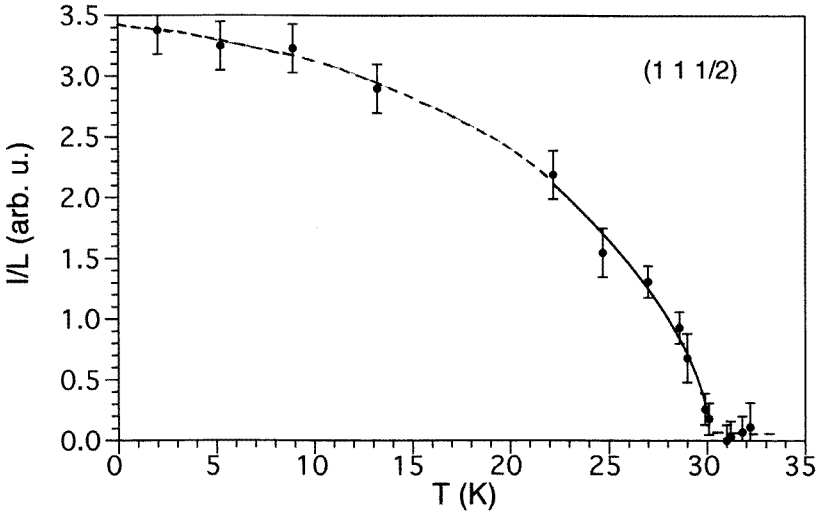

Figure 3. The temperature dependence of the intensity of the $(1, 1, 1/2)$ magnetic Bragg reflection. The solid line is a fit of the power law $I/I_0 = (1 - T/T_N)^{2\beta}$ near T_N.

Table 2. Neutron scattering intensities of the measured magnetic Bragg reflections and magnetic scattering amplitudes calculated from the measured data for the Γ_8 configuration. I/L: the Lorentz-corrected scattered intensity; $|G_{hkl}|^2$: the squared moduli of the geometrical structure factor; $q^2 = \langle \sin^2 \alpha \rangle$, where α is the angle between the direction of the moments and the momentum transfer; μf: the magnetic scattering amplitude (μ_B/U); μ: the magnetic moment of the U atoms (μ_B) assuming a U^{3+} form factor.

			Γ_8		Γ_{10}	
hkl	I/L	$\lvert G_{hkl}\rvert^2$	$\langle \sin^2 \alpha \rangle$	μf	$\langle \sin^2 \alpha \rangle$	μf
1 0 1/2	0.97(3)	3.513	0.481	0.50	0.760	0.39
3 0 1/2	5.8(2)	15.815	0.893	0.42	0.553	0.54
5 0 1/2	0.72(17)	6.689	0.959	0.22	0.521	0.30
1 1 1/2	3.21(14)	9.745	0.649	0.47	0.675	0.46
2 1 1/2	0.46(4)	1.105	0.822	0.46	0.588	0.55
5 1 1/2	1.0(2)	7.266	0.960	0.25	0.520	0.34
2 2 1/2	2.7(2)	7.518	0.881	0.42	0.559	0.52
3 2 1/2	1.40(17)	4.974	0.923	0.36	0.538	0.48
4 2 1/2	2.2(3)	9.458	0.949	0.33	0.526	0.44
3 0 3/2	2.04(13)	15.815	0.481	0.34	0.760	0.27
1 1 3/2	0.62(8)	9.744	0.171	0.40	0.915	0.17
2 2 3/2	1.07(9)	7.518	0.452	0.37	0.774	0.28
3 2 3/2	1.0(3)	4.974	0.572	0.39	0.714	0.35
4 2 3/2	1.0(2)	9.458	0.673	0.26	0.664	0.27

structures compatible with a given crystallographic group. Irreducible-representation analysis is one of such tools introduced by Bertaut *et al* (1968) that has proven to be helpful in interpreting neutron diffraction patterns of magnetic compounds.

Bourée *et al* (1994) derived all possible magnetic structures with wave-vector $\boldsymbol{k} = (0, 0, 1/2)$ for the 2:2:1 compounds crystallizing in the space group $P4/mbm$. There are ten

distinct irreducible representations of the magnetic group, two of those having a zero moment on the actinide site fixed by symmetry. From the remaining eight irreducible representations, four configurations ($\Gamma_1, \Gamma_3, \Gamma_5$ and Γ_7) correspond to non-collinear magnetic structures. From the subset of collinear structures, three ($\Gamma_2, \Gamma_8, \Gamma_9$) have moments parallel to the ***c***-axis and one has moments in the *a–b* plane (Γ_{10}). The reader is referred to the paper of Bourée *et al* for more details on the irreducible-representation analysis of the symmetry-allowed magnetic structures of these types of compound.

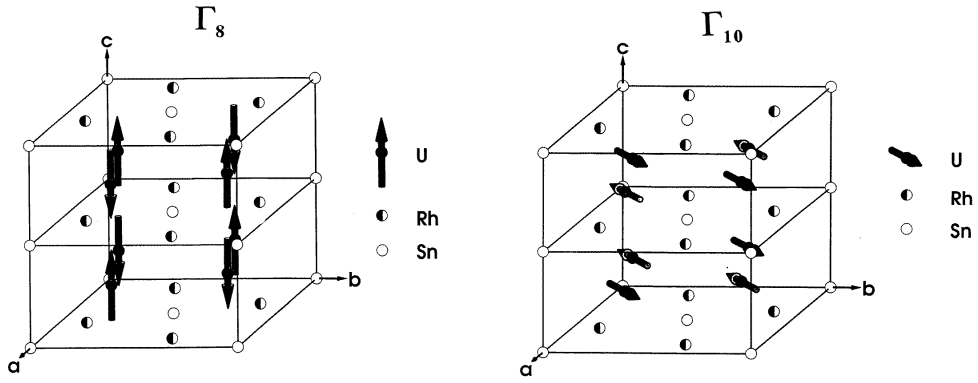

Figure 4. Magnetic structures corresponding to the Γ_8 and Γ_{10} irreducible representation of the magnetic space group of U_2Rh_2Sn. Note that the magnetic unit cell doubles the nuclear unit cell along the ***c***-axis and includes two layers of uranium atoms with the directions of their spins reversed. For Γ_{10}, the in-plane angle between the direction of the moments and the ***a***-axis is not fixed by symmetry and its value cannot be determined from the neutron diffraction pattern for either a multi-domain single-crystalline or a polycrystalline sample. This figure was drawn with this angle fixed at 45°.

The neutron powder diffraction measurements of Nakotte *et al* (1996) have shown that the most likely magnetic structure of U_2Rh_2Sn will correspond to either the Γ_8 or Γ_{10} configuration. These two types of magnetic structure are shown in figure 4. Unfortunately, the small value of the ordered moment in U_2Rh_2Sn severely limited the amount of information that could be extracted from such an experiment. In fact, Nakotte *et al* could measure only two magnetic reflections (1, 0, 1/2) and (1, 1, 1/2) with significant statistical accuracy above the background level. These two strong reflections are compatible only with the Γ_8 or Γ_{10} types of magnetic ordering. A Rietveld refinement of the low-temperature diffraction pattern including five additional weak magnetic reflections with $I < 2\sigma$ gave a marginally better fit for the Γ_8 configuration that has the moments pointing along the ***c***-axis ($\chi^2 = 0.7$ for Γ_8 and $\chi^2 = 1.4$ for Γ_{10}). The refined value of the magnetic moment was 0.38(1) μ_B/U atom.

A much higher peak-to-background ratio can be obtained in a single-crystal experiment and we will show below that sufficient data could be measured in our single-crystal neutron experiment to effectively discriminate between the two types of magnetic ordering.

For a collinear magnetic structure like Γ_8 or Γ_{10}, the intensities of the magnetic Bragg reflections are given by

$$I_{hkl}/L = Syp^2(\mu f(Q))_U^2 \langle \sin^2 \alpha \rangle |G_{hkl}|^2 \, \mathrm{e}^{-2W} \tag{1}$$

where μ is the magnetic moment of the uranium atoms, $f(Q)$ the associated form factor and α is the angle between the magnetic moment and the scattering vector $\boldsymbol{Q}$

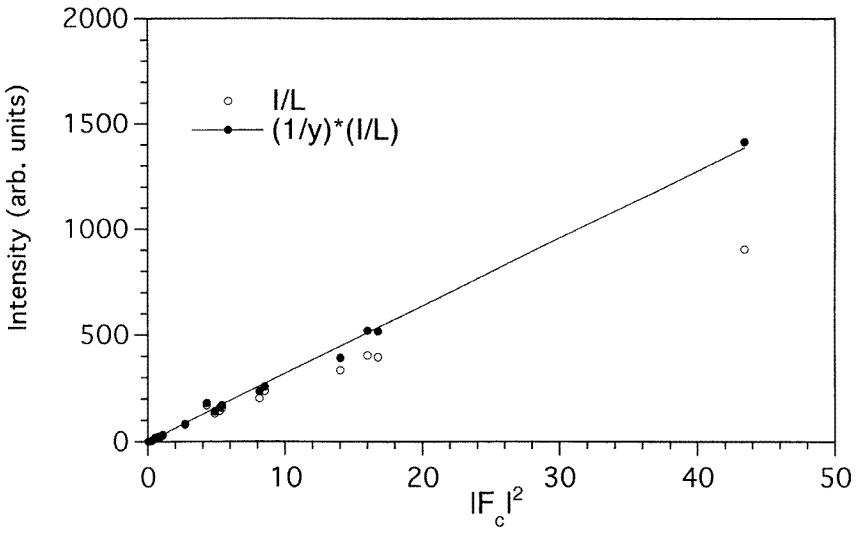

Figure 5. A plot of the integrated intensities of the nuclear Bragg reflections versus the square of their nuclear structure factors. The open symbols correspond to the intensities before extinction correction and the solid symbols to the extinction-corrected intensities. The line represents the best fit to the latter values and its slope is the scale factor $S = 32.0(5)$.

($|\boldsymbol{Q}| = 4\pi(\sin\theta)/\lambda$) (Rossat-Mignod 1987). S and y are the instrumental scale factor and the extinction correction, respectively. The numerical factor $p = 0.2695$ is the neutron scattering length (in units of 10^{-12} cm) associated with 1 μ_B, and e^{-2W} is the conventional Debye–Waller factor. The geometrical structure factor, G_{hkl}, accounts for the mutual interference of the scattered neutron beam within the magnetic sublattice:

$$G_{hkl} = \sum_j s_j e^{2\pi i(hx_j + ky_j + lz_j)} \tag{2}$$

where summation extends over the magnetic atoms of the unit cell and $s_j = \pm 1$ for spins up $(+1)$ or down (-1). For both Γ_8 and Γ_{10} magnetic structures that have the same configurational symmetry (i.e. that have the same pattern of $+$ and $-$ spins although with different spin directions)

$$|G_{hkl}|^2 = \begin{cases} (4\sin(2\pi hx)\sin(2\pi kx))^2 & h+k \text{ even} \\ (4\cos(2\pi hx)\cos(2\pi kx))^2 & h+k \text{ odd.} \end{cases} \tag{3}$$

For a uniaxial structure it can be shown (Shirane 1959) that the average of the angular factor $\sin^2\alpha$ over the orientation domains in a multi-domain sample is a function only of the angle φ between the direction of the magnetic moments and the unique axis. For a tetragonal structure,

$$\langle \sin^2\alpha \rangle = 1 - \left\{ \frac{1}{2}\frac{h^2+k^2}{a^2}\sin^2\varphi + \frac{l^2}{c^2}\cos^2\varphi \right\} d_{hkl}^2 \tag{4}$$

where d_{hkl} is the interplanar distance of the (hkl) lattice planes originating the Bragg reflection. In particular, when the moments are oriented along $\boldsymbol{c}$ as in $\Gamma_8(\varphi = 0)$ or lying

in the basal plane as in $\Gamma_{10}(\varphi = \pi/2)$, the previous expression reduces to the simpler forms

$$\begin{aligned} \boldsymbol{\mu} \parallel \boldsymbol{c}: \qquad & \langle \sin^2 \alpha \rangle = \frac{h^2 + k^2}{h^2 + k^2 + l^2(a/c)^2} \\ \boldsymbol{\mu} \perp \boldsymbol{c}: \qquad & \langle \sin^2 \alpha \rangle = \frac{\frac{1}{2}(h^2 + k^2) + l^2(a/c)^2}{h^2 + k^2 + l^2(a/c)^2}. \end{aligned} \tag{5}$$

It is clear from the discussion above that the intensities of the magnetic Bragg reflections for a given value of ordered magnetic moment will differ for the two types of magnetic ordering shown in figure 4 because the value of $\langle \sin^2 \alpha \rangle$ for each reflection is different in the two cases.

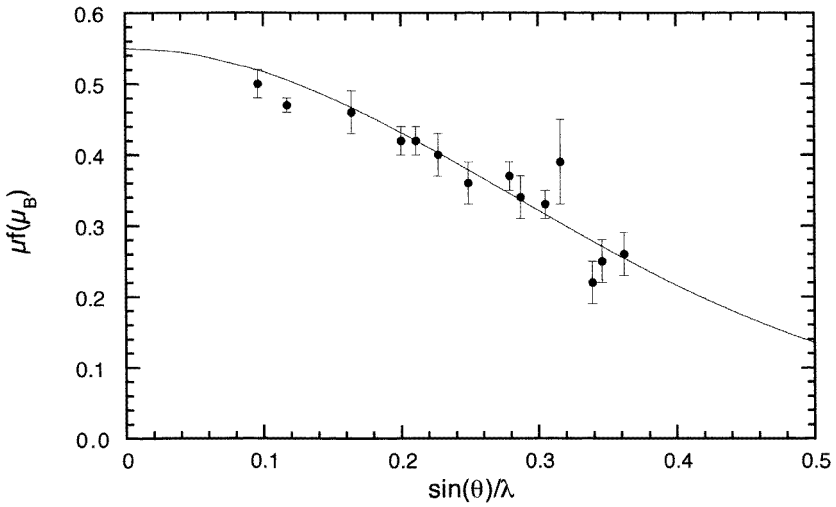

Figure 6. The magnetic scattering amplitude of the uranium atom derived from the experimental values using equation (1) plotted as a function of $(\sin\theta)/\lambda$. The solid line represents a fit to the U^{3+} form factor in the dipole approximation.

In order to determine the value of the ordered magnetic moment, the intensities of the magnetic Bragg reflections have to be given on an absolute scale. The scale factor was determined by measuring the intensities of a set of 25 nuclear reflections. These were corrected for $\lambda/2$ contamination and for extinction using the Becker and Coppens (1974) model with the parameters refined from the four-circle data. The corrected intensities were plotted versus the square of the nuclear structure factor in order to determine the scale factor (figure 5). From this plot, a linear regression gives a value of $S = 32.0(5)$ for the scale factor. One can then use equation (1) to determine the magnetic scattering amplitude μf of each uranium atom. As the magnetic form factor $f(Q)$ usually decreases regularly with the momentum transfer, one expects the magnetic scattering amplitude derived from equation (1) to be a smooth function of $(\sin\theta)/\lambda$ *if* the correct magnetic structure is used to calculate the values of the geometric structure factors and $\langle \sin^2 \alpha \rangle$. The values of μf for the Γ_8 and Γ_{10} magnetic structure are given in table 2 and a plot of μf versus $(\sin\theta)/\lambda$ for Γ_8 is shown in figure 6.

A least-squares fit of the magnetic structure with respect to the measured magnetic intensities using equation (1) was performed for both the Γ_8 and Γ_{10} types of magnetic ordering. Although it was found for other uranium intermetallics with rhodium that

hybridization between the f electrons and the d band can induce a significant magnetic moment at the transition metal site (Paixão *et al* 1992), it was assumed as a first approximation that the magnetic moment is carried only by the actinide atoms. The magnetic form factor of the uranium atoms was calculated in the dipole approximation (Marshall and Lovesey 1971):

$$\mu f(Q) = \mu(\langle j_0\rangle + C_2\,\langle j_2\rangle) \qquad C_2 = \frac{\mu_L}{\mu} \tag{6}$$

with the ratio between the orbital (μ_L) and total moment (μ) fixed at the theoretical value for a free U^{3+} ion. For an intermediate-coupling configuration corresponding to the spectroscopic g-value of the free ion, $C_2 = 1.64$. We used the $\langle j_0\rangle$- and $\langle j_2\rangle$-functions calculated by Desclaux and Freeman (1978) for the U^{3+} state.

Table 3. Observed intensities (corrected by the Lorentz factor) and calculated intensities for the best least-squares fit of the Γ_8 and Γ_{10} magnetic structures.

hkl	I_{obs}	$I_{calc}(\Gamma_8)$	$I_{calc}(\Gamma_{10})$
1 0 1/2	0.97(3)	0.984	0.885
3 0 1/2	5.8(2)	5.359	1.892
5 0 1/2	0.72(7)	1.055	0.326
1 1 1/2	3.21(14)	3.491	2.068
2 1 1/2	0.46(4)	0.427	0.174
5 1 1/2	1.0(2)	1.090	0.336
2 2 1/2	2.7(2)	2.651	0.959
3 2 1/2	1.40(17)	1.410	0.468
4 2 1/2	2.2(3)	1.910	0.603
3 0 3/2	2.04(13)	1.830	1.647
1 1 3/2	0.62(8)	0.579	1.766
2 2 3/2	1.07(9)	0.861	0.841
3 2 3/2	1.0(3)	0.557	0.395
4 2 3/2	1.0(2)	0.870	0.489

The best fit was obtained for the Γ_8 representation of the magnetic group, for which a final χ^2-value of 1.9 was obtained. The refined value of the magnetic moment of each uranium atom was 0.53(2) μ_B. A similar fit with the Γ_{10} type of magnetic order gave a much poorer fit with a minimum χ^2 of 68 for $\mu_U = 0.4\ \mu_B$/atom. The results of the least-squares fits are given in table 3. It should be pointed that the moment found for the magnetic structure is higher than that obtained by Nakotte *et al* from the Rietveld refinement of their powder spectrum, using the same spin configuration. However, Nakotte *et al* acknowledge that with the reduced number of magnetic reflections in their powder data, the value for the uranium moment obtained from the Rietveld refinement has to be treated with caution.

4. Discussion

Both the temperature and the field dependencies of the magnetization indicate an antiferromagnetic order of the uranium atoms along the ***c***-direction, with a Néel temperature $T_N = 28(2)$ K. This was confirmed by the neutron scattering data collected for a single crystal, unambiguously showing that the U_2Rh_2Sn orders in a magnetic structure corresponding to the Γ_8 representation of the space group with $k = (0, 0, 1/2)$. Our single-crystal study is in agreement with that of Nakotte *et al* (1996) performed on a polycrystalline sample. The fact that the uranium moments in U_2Rh_2Sn point along the

$\boldsymbol{c}$-axis constitutes an exception to the rule that the f moments should point perpendicularly to the shortest f–f bond distances, as in this compound the shortest interuranium distances ($d_{f-f} = 3.63$ Å) are found to lie along the easy axis. The magnetic anisotropy of this compound is nevertheless relatively large as shown both by susceptibility and high-field magnetization measurements. It should be pointed out that this anisotropy is manifested even in the paramagnetic state: with $\boldsymbol{H} \parallel \boldsymbol{c}$ the susceptibility follows a Curie–Weiss law with $\theta = -105(2)$ K and $\mu_{eff} = 2.80\ \mu_B$/U, while in the perpendicular direction a modified Curie–Weiss law is observed with the parameters θ and μ_{eff} reduced by a factor of $\approx 1/2$. This difference between the behaviours in the two directions reflects the importance of the anisotropy in the paramagnetic region. The origin of the magnetic anisotropy in the An_2T_2X family of compounds deserves closer investigation. It is not unlikely that hybridization effects between the f electrons and the ligands, like those found in the 1:1:1 compounds, could contribute significantly to the anisotropy. This study does not show evidence for a moment at the Rh site, as the U form factor derived assuming a zero moment on the Rh atoms follows a reasonably smooth curve. However, a detailed and more precise investigation of the magnetization density distribution using polarized neutrons would be worthwhile although such an experiment would have to be done above T_N, probing the small induced magnetization aligned with the field.

Acknowledgments

We are indebted to G H Lander for encouraging this work and for his comments on the manuscript. L C J Pereira acknowledges the European Commission (EC) for support given in the framework of the 'Human Capital and Mobility' programme. J A Paixão and L C J Pereira gratefully acknowledge support for the neutron experiments at Siloë given in the framework of the Large Installations Programme of the EC. This work was partially supported by JNICT under contracts No PRAXIS/3/3.1/FIS/29/94 and No PBIC/FIS/2213/95 and by NATO through the Collaborative Research Grant 920996.

References

Becker P J and Coppens P 1974 *Acta Crystallogr.* A **30** 129
Bertaut E F 1968 *Acta Crystallogr.* A **24** 217
Bourée F, Chevalier B, Fournès L, Mirambet F, Roisnel T, Tran V H and Zolnierek Z 1994 *J. Magn. Magn. Mater.* **138** 307
Brown P J and Matthewman J C 1987 The Cambridge crystallographic subroutine library—Mark 3 user's manual *Rutherford Appleton Laboratory Internal Report* RAL-87-010
Desclaux J P and Freeman A J 1978 *J. Magn. Magn. Mater.* **8** 119
Divis M, Olsovec M, Richter M and Eschrig H 1995 *J. Magn. Magn Mater.* **140–144** 1365
Divis M, Richter M and Eschrig H 1994 *Solid State Commun.* **90** 99
Fukushima T, Matsuyama S, Kumada T, Kindo K, Prokes K, Nakotte H, de Boer F R, Havela L, Sechovsky V, Winand J M, Rebizant J and Spirlet J C 1995 *Physica* B **211** 142
Havela L, Sechovsky V, Svoboda P, Nakotte H, Prokes K, de Boer F R, Seret A, Winand J M, Rebizant J, Spirlet J C, Purwanto A and Robinson R A 1995 *J. Magn. Magn. Mater.* **140–144** 1367
Koester L, Rauch H and Seymann E 1991 *At. Data Nucl. Data Tables* **49** 65
Lehmann M S and Larson F K 1974 *Acta Crystallogr.* A **30** 580
Marshall W and Lovesey S W 1971 *Theory of Neutron Scattering From Condensed Matter* (London: Oxford University Press)
McClandish L E, Stout G H and Andrews L C 1975 *Acta Crystallogr.* A **31** 245
Mirambet F, Chevalier B, Fournès L, Gravereau P and Etourneau J 1994 *J. Alloys Compounds* **203** 29
Mirambet F, Gravereau P, Chevalier B, Trut L and Etourneau J 1993 *J. Alloys Compounds* **191** L1

Nakotte H, Prokes K, Brück E, Tang N, de Boer F R, Svoboda P, Sechovsky V, Havela L, Winand J M, Seret A, Rebizant J and Spirlet J C 1994 *Physica* B **201** 247

Nakotte H, Purwanto A, Robinson R A, Prokes K, Klaasse J C P, Châtel P F, de Boer F R, Havela L, Sechovsky V, Pereira L C J, Seret A, Rebizant J, Spirlet J C and Trouw F 1996 *Phys. Rev.* B **53** 3263

Paixão J A, Delapalme A, Lander G H, Brown P J, Nakotte H, de Boer F R and Brück E 1993 *Europhys. Lett.* **24** 607

Paixão J A, Lander G H, Brown P J, Nakotte H, de Boer F R and Brück E 1992 *J. Phys.: Condens. Matter* **4** 829

Pereira L C J, Winand J M, Wastin F, Rebizant J and Spirlet J C 1995 *25ièmes Journées des Actinides (L'Aquila, Italy)* abstract 124

Péron M N, Kergadallan Y, Rebizant J, Meyer D, Winand J M, Zwirner S, Havela L, Nakotte H, Spirlet J C, Kalvius G M, Colineau E, Oddou J L, Jeandey C and Sanchez J P 1993 *J. Alloys Compounds* **201** 203

Rossat-Mignod J 1987 *Methods of Experimental Physics* vol 23c, ed K Sköld and L Price (New York: Academic)

Sechovsky V and Havela L 1988 *Ferromagnetic Materials* vol IV, ed E P Wohlfarth and K H G Buschow (Amsterdam: North-Holland)

Shirane G 1959 *Acta Crystallogr.* **12** 282